




## Article

# Study of the adsorption mechanisms of NH<sub>3</sub>, H<sub>2</sub>S and SO<sub>2</sub> on sepiolite using molecular dynamics simulations

Ji Zhou<sup>1,2</sup>, Zuozhang Wang<sup>2</sup>, Ana C.S. Alcântara<sup>3</sup> and Yanhuai Ding<sup>1,2\*</sup> 

<sup>1</sup>College of Civil and Environmental Engineering, Hunan University of Science and Engineering, Yongzhou, 425199, China; <sup>2</sup>Institute of Rheological Mechanics, Xiangtan University, 411105, Xiangtan, Hunan, China and <sup>3</sup>Department of Chemistry, Universidade Federal do Maranhão, 65080-805 São Luís - MA, Brazil

### Abstract

The adsorption mechanisms of hazardous gas molecules such as NH<sub>3</sub>, H<sub>2</sub>S and SO<sub>2</sub> on sepiolite have not yet been elucidated. Therefore, molecular dynamics (MD) simulations were employed to investigate the adsorption behaviour of sepiolite towards NH<sub>3</sub>, H<sub>2</sub>S and SO<sub>2</sub>. A calculation model for sepiolite containing structural and zeolitic water molecules was constructed in this study. The adsorption sites and molecular configurations of the hazardous gases in the sepiolite channels were studied. The radial distribution function was employed to evaluate the interactions between the gas molecules and sepiolite. The results show that the order of adsorption capacity of sepiolite for the gases is as follows: SO<sub>2</sub> > H<sub>2</sub>S > NH<sub>3</sub>. These three types of gas molecules absorbed in the channel nanopores of sepiolite exhibit different atomic configurations. The diffusion coefficients of the gas molecules in the channels decreased in the following order: NH<sub>3</sub> > H<sub>2</sub>S > SO<sub>2</sub>. In addition, the diffusion coefficients were affected significantly by the ratio of the number of gas/water molecules. This study provides new perspectives for understanding the molecular processes responsible for the adsorption properties of sepiolite.

**Keywords:** adsorption mechanism, H<sub>2</sub>S, molecular dynamics, NH<sub>3</sub>, sepiolite, SO<sub>2</sub>

(Received 10 May 2022; revised 31 August 2022; Accepted Manuscript online: 12 September 2022; Associate Editor: Chun Hui Zhou)

As a natural mineral, sepiolite has many industrial applications related specifically to its physical properties (Zheng *et al.*, 2010; Deng *et al.*, 2019; Jiang *et al.*, 2020, 2021; Hamid *et al.*, 2021). Due to their inherently large surface areas (~320 m<sup>2</sup> g<sup>-1</sup>) and great adsorption capacities, sepiolite-based materials have shown great potential for applications in the fields of environmental clean-up and protection (Alcântara *et al.*, 2012; Fayazi *et al.*, 2019; Bashir *et al.*, 2020). Sepiolite is a microcrystalline hydrated magnesium silicate hydrate that belongs to the phyllosilicate family. It has a unit cell formula of Si<sub>12</sub>O<sub>30</sub>Mg<sub>8</sub>(OH)<sub>4</sub>(H<sub>2</sub>O)<sub>4</sub>·8H<sub>2</sub>O. This silicate is composed of continuous silica tetrahedral chains with the apical oxygen inverted periodically. Furthermore, discontinuous octahedral sheets are constructed in the [010] direction, thereby forming channels parallel to the *c*-axis of the crystal (García-Romero & Suárez, 2013, 2018; Lu & Wang, 2022). The channel structure provides sepiolite with a very large specific surface area, potentially diversifying its advanced applications (Qiu *et al.*, 2021; Erdoğan & Esenli, 2022). In addition, due to its nano-channels with a size range of 0.6–0.9 nm, sepiolite has been classified as a molecular sieve material (Alver, 2018; Cecilia *et al.*, 2018). Therefore, sepiolite could be used as an active component for the adsorption of various small polar molecules (Delgado *et al.*, 2007; Yuan *et al.*, 2018). Experimental results have indicated the dependence of the gas adsorption of sepiolite on molecule size as well as on the interactions between the molecules and the channel walls.

Acid treatment has been used widely to improve the adsorption properties of sepiolite (Yebra-Rodríguez *et al.*, 2003). Acid-activated sepiolite exhibited weak acidity and small  $\zeta$ -potential values, indicating the dominance of Lewis acid centres on its surface (Sabah *et al.*, 2007). The special affinity of sepiolite towards NH<sub>3</sub> indicated the occurrence of specific interactions with the acid groups on its surface. Although the adsorption behaviour of sepiolite has been studied widely, the molecular mechanism underlying the impacts of hazardous gases such as NH<sub>3</sub>, H<sub>2</sub>S and SO<sub>2</sub> on the adsorption behaviour of sepiolite has not yet been resolved. Due to the limitations of experimental technologies, the interactions between these hazardous gas molecules and sepiolite cannot be measured directly. However, molecular dynamics (MD) simulations can provide more precise microscopic information on sepiolites compared to experimental methods.

The distribution and dynamics of the confined water in the channel nanopores of sepiolite have been investigated using MD simulations (Zhou *et al.*, 2016). Based on these results, a new zeolitic water model was proposed to study the water mobility in these channels. Herein, the MD simulation method was employed to investigate the adsorption mechanism of NH<sub>3</sub>, H<sub>2</sub>S and SO<sub>2</sub> on sepiolite. The adsorption sites and molecular configurations of the hazardous gases in the sepiolite channels were studied. This study provides new research insights and methods for studying the application of sepiolite materials.

### Experimental

#### Simulation structure of sepiolite

The molecular models of sepiolite shown in Fig. 1 were constructed according to previous studies (Muniz-Miranda *et al.*,

\*Email: yhding@xtu.edu.cn

Cite this article: Zhou J, Wang Z, Alcântara ACS, Ding Y (2022) (2023). Study of the adsorption mechanisms of NH<sub>3</sub>, H<sub>2</sub>S and SO<sub>2</sub> on sepiolite using molecular dynamics simulations. *Clay Minerals* 58, 1–6. <https://doi.org/10.1180/clm.2022.22>

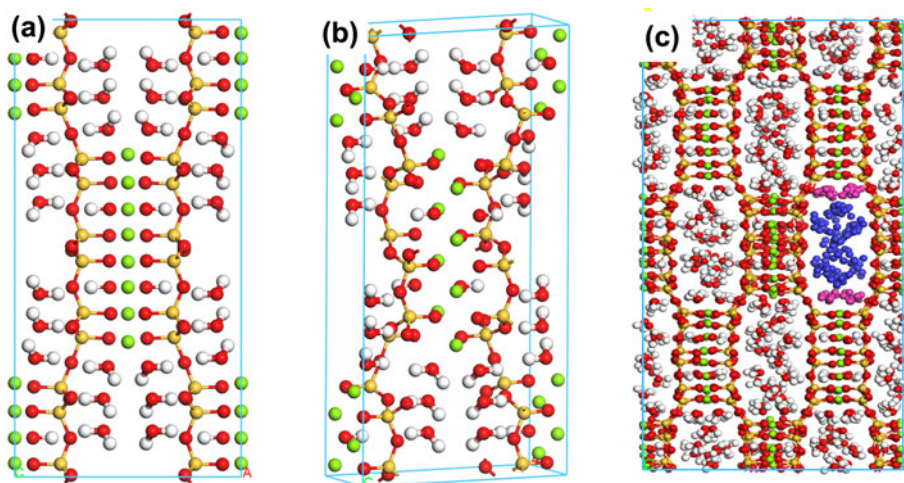


**Fig. 1.** Computational models of sepiolite. The Si, O, Mg and H atoms are represented in yellow, red, green and grey, respectively. The pink and blue atomic clusters indicate structural water and zeolitic water, respectively. (a) The atomic configuration of the cell before simulation. (b) The atomic configuration of the cell after a relaxation process. (c) The atomic configuration of the supercell in the MD simulation.

2016; Zhou *et al.*, 2016). The calculation model was based on the molecular formula  $\text{Mg}_8(\text{Si}_{12}\text{O}_{30})(\text{OH})_4(\text{OH}_2)_4 \cdot n\text{H}_2\text{O}$ , where  $n$  indicates the number of zeolitic water molecules in the calculated system (Kitayama & Hayakawa, 1992; Suárez & García-Romero, 2013). The  $\text{H}_2\text{O}$  molecules in sepiolite can be classified into two groups after structure optimization: (1)  $\text{H}_2\text{O}$  molecules that are bonded strongly to  $\text{Mg}^{2+}$  ions located at the edges of octahedral sheets, corresponding to the structural water reported in previous studies (Balci, 1999; Fitaroni *et al.*, 2019); and (2)  $\text{H}_2\text{O}$  molecules that form hydrogen bonds between themselves, called ‘zeolitic water molecules’ (Cornejo & Hermosin, 1988; Balci, 1999). The calculated system, containing zeolitic water molecules, is shown in Fig. 1c. Water molecules were located in the channels inside sepiolite.

The adsorption of gas molecules into sepiolite channels was simulated by constructing a computational model. The computational model contained 160 structural water molecules and 320 zeolitic water molecules. Owing to the high stability of the structural water, these molecules were maintained in the channels throughout the simulation process. Following this, a portion of the zeolitic water molecules was substituted artificially with the gas molecules. The ratios of the number of gas/water molecules ( $\chi_i$ ) are listed in Table 1.

### Forcefield setup and MD parameters

The MD simulation was performed using the *Forcite* module in *BIOVIA Material Studio 2017 R2*. All simulations were performed by using the fully atomistic COMPASS II forcefield (Sun *et al.*, 2014; He *et al.*, 2020). Equilibration was performed in a canonical ensemble at 300 K with a time constant of  $1 \times 10^{-15}$  s. Pre-equilibration procedures ( $100 \times 10^{-20}$  s) were performed to

**Table 1.** Ratios of the numbers of gas/water molecules ( $\chi_i$ ) in the channels of the computational model.

No. of $\text{H}_2\text{O}$ molecules	480	400	320	240	160
Structural $\text{H}_2\text{O}$	160	160	160	160	160
Zeolitic $\text{H}_2\text{O}$	320	240	160	80	0
Gas molecules ( $\text{NH}_3$ , $\text{H}_2\text{S}$ , $\text{SO}_2$ )	0	80	160	240	320
Gas/ $\text{H}_2\text{O}$ ratio	$\chi_0 = 0$	$\chi_1 = 0.2$	$\chi_2 = 0.5$	$\chi_3 = 1.0$	$\chi_4 = 2.0$

ensure that the system reached the equilibrium state. The simulations were performed for  $\sim 3 \times 10^{-12}$  s with a time step of  $2 \times 10^{-15}$  s. The atom coordinates were saved every  $1 \times 10^{-15}$  s.

### Results and discussion

The distributions of adsorbed gas molecules in the channels of sepiolite are shown in Fig. 2. The coordinate origin was placed at the centre of the channel. At various values of  $\chi_i$ , sepiolite showed similar adsorption behaviour towards  $\text{NH}_3$  in the  $x$ - and  $y$ -directions (Fig. 2a,d). These results indicate that the number of zeolitic water molecules had a minor effect on the adsorption of  $\text{NH}_3$  molecules. The distributions of the  $\text{NH}_3$  molecules in the channels were symmetrical in the  $x$ - and  $y$ -directions. The adsorption peaks were located at 0.5 and 1.4 Å from the centre of the channels in the  $x$ -direction and at 2.5 and 4.5 Å from the centre of the channels in the  $y$ -direction. For  $\text{H}_2\text{S}$  (Fig. 2b,e), the molecular distribution changed with increasing  $\chi_i$  values. In the  $x$ -direction, the adsorption peak was located at the centre of the channel at  $\chi_1 = 0.2$  before disappearing at  $\chi_1 = 0.5$ . Two adsorption peaks were observed at 1.5 Å from the centre of the channel. Four adsorption peaks were observed at  $\chi_3 = 1$  and  $\chi_4 = 2$ . In the  $y$ -direction, the molecular distribution of  $\text{H}_2\text{S}$  exhibited a similar shape at various  $\chi_i$  values. For  $\text{SO}_2$  (Fig. 2c,f), the molecular distribution was affected by the value of  $\chi_i$  in the  $x$ - and  $y$ -directions. The results obtained indicated that the molecular configuration of the gases in the channels was determined by both  $\chi_i$  and the interactions between the gas molecules and sepiolite. The adsorbed gas molecules in the channels were distributed symmetrically.

The radial distribution function (RDF) was employed to evaluate the interaction between gas molecules and sepiolite (Abbaspour *et al.*, 2018; Lamichhane & Ghimire, 2021). For  $\text{NH}_3$  adsorption, the N–N, N– $\text{O}_w$ , N–Si, Mg– $\text{O}_w$ , Si– $\text{O}_w$  and N– $\text{O}_s$  distances are presented in Fig. 3, where  $\text{O}_w = \text{O}$  atoms in zeolitic water molecules and  $\text{O}_s = \text{O}$  atoms in structural water molecules. The RDFs of N–N and N– $\text{O}_s$  in Fig. 3a,f show a similar pattern. The peaks were located at  $\sim 3.2$  Å, indicating that  $\text{NH}_3$  molecules exhibited the same level of affinity towards the nearest N and Si atoms. The RDF in Fig. 3b demonstrates a stronger N– $\text{O}_w$  interaction compared to N–N and N– $\text{O}_s$  interactions. The  $\text{NH}_3$  molecules exhibited a weak interaction with the Si atoms. Therefore, the  $\text{NH}_3$  adsorption of sepiolite can be

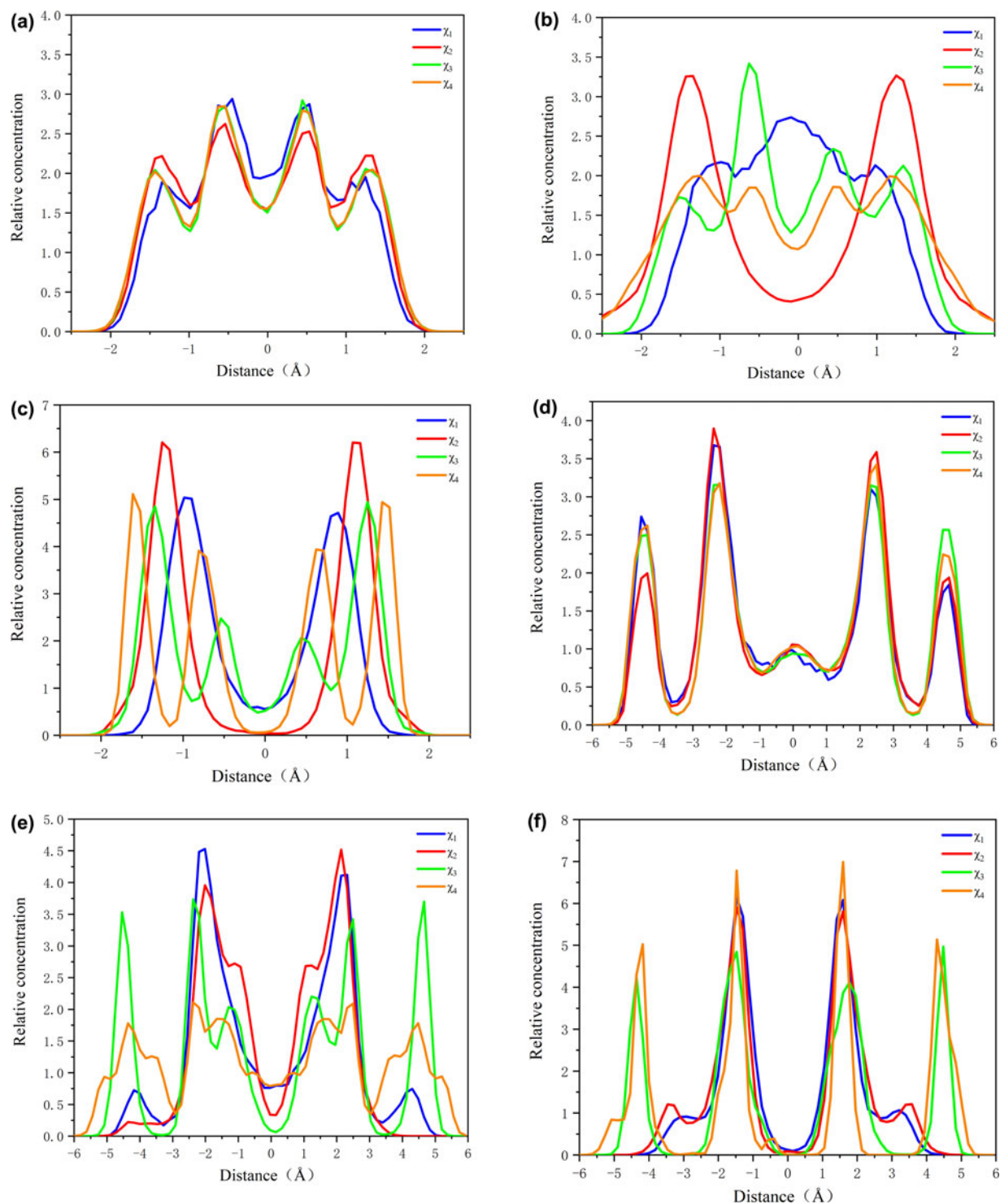


**Fig. 2.** Distribution of the adsorbed gas molecules in the channels. (a,d) Distribution of  $\text{NH}_3$  in the x- and y-directions. (b,e) Distribution of  $\text{H}_2\text{S}$  in the x- and y-directions. (c,f) Distribution of  $\text{SO}_2$  in the x- and y-directions.

increased *via* the interaction between  $\text{NH}_3$  and zeolitic water molecules. The complicated adsorption process is associated with the number of zeolitic water molecules. However, the structural water molecules were bonded tightly to the  $\text{Mg}^{2+}$  in the sepiolite, producing only a small decrease in  $\text{NH}_3$  adsorption. The results in Fig. 3 indicate that the N-N, N- $\text{O}_w$ , N-Si, Mg- $\text{O}_w$ , Si- $\text{O}_w$  and N- $\text{O}_s$  interactions were not affected significantly

by the change in  $\chi_i$ . For  $\text{H}_2\text{S}$  (Fig. S1), the S- $\text{O}_w$  distance was very similar to the S- $\text{O}_s$  distance, indicating that the  $\text{H}_2\text{S}$  molecules interacted identically with the O atoms in both zeolitic and structural water molecules. In comparison, the  $\text{SO}_2$  molecules (Fig. S2) exhibited a high affinity to the O atoms in the structural water but not in the zeolitic water. The interactions among the  $\text{SO}_2$  molecules increased with the decreasing number of zeolitic

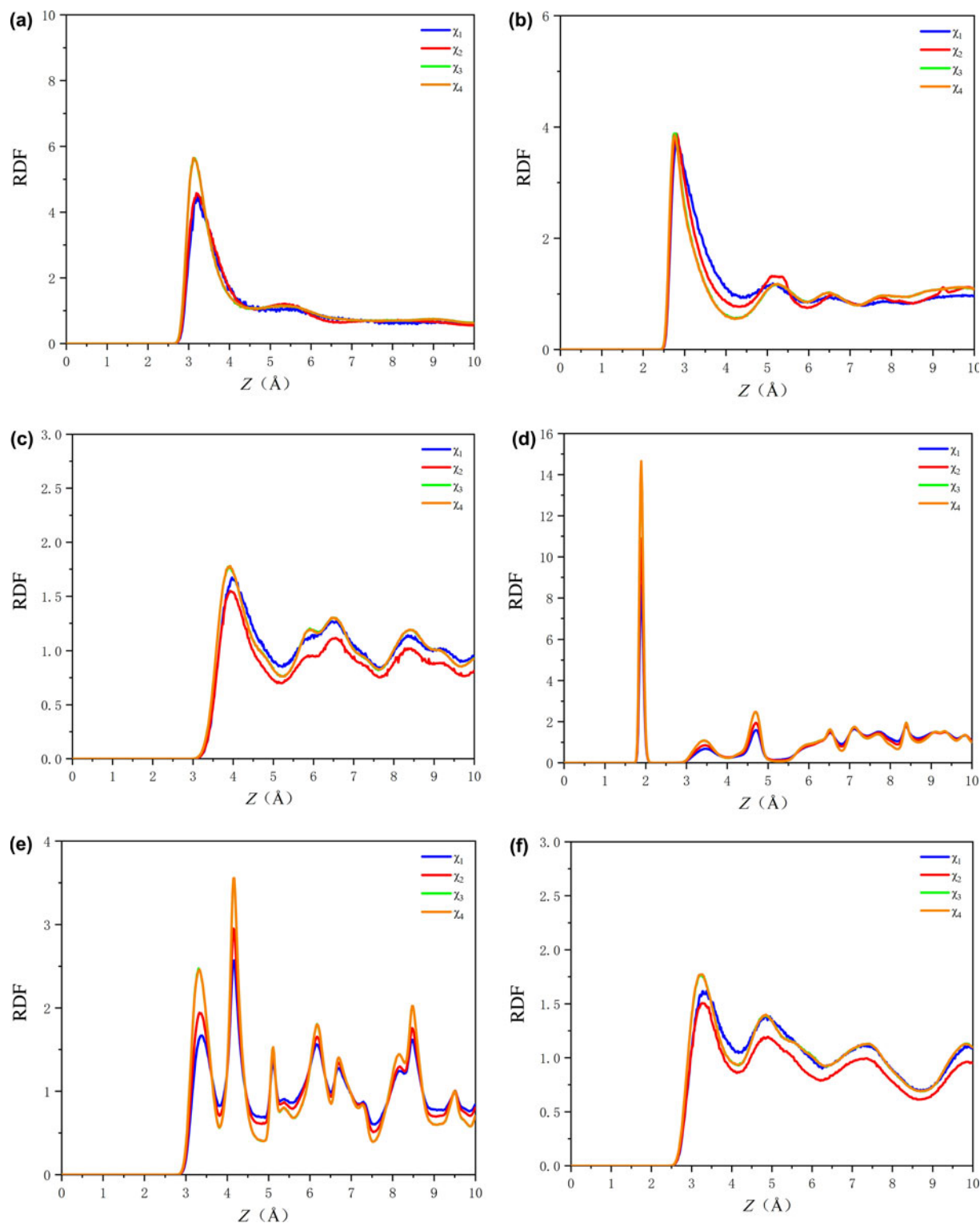


**Fig. 3.** RDF patterns of  $\text{NH}_3$  adsorption with various values of  $\chi_i$ , wherein N indicates the N atoms in  $\text{NH}_3$ ,  $\text{O}_w$  is the O atoms in zeolitic water molecules, Si and Mg indicate the Si and Mg atoms in sepiolite and  $\text{O}_s$  indicates the O atoms in structural water molecules. (a) N-N; (b) N- $\text{O}_w$ ; (c) N-Si; (d) Mg- $\text{O}_w$ ; (e) Si- $\text{O}_w$ ; and (f) N- $\text{O}_s$ .  $Z$  = distance between the atoms.

molecules. These results demonstrate that the  $\text{SO}_2$  molecules tended to adsorb onto the channel walls, indicating the stability of  $\text{SO}_2$  molecules adsorbed on sepiolite.

In the absence of zeolitic water in the channel, the structural water molecules were bound tightly to the  $\text{Mg}^{2+}$  during the

simulation process for both  $\text{H}_2\text{S}$  and  $\text{SO}_2$  (Fig. 4). However, during the adsorption of  $\text{NH}_3$ , some of the bonds between the structural water molecules and  $\text{Mg}^{2+}$  were broken, and so the water molecules interacted with the  $\text{NH}_3$  molecules. In addition, the adsorbed gas molecules in the channels exhibited various



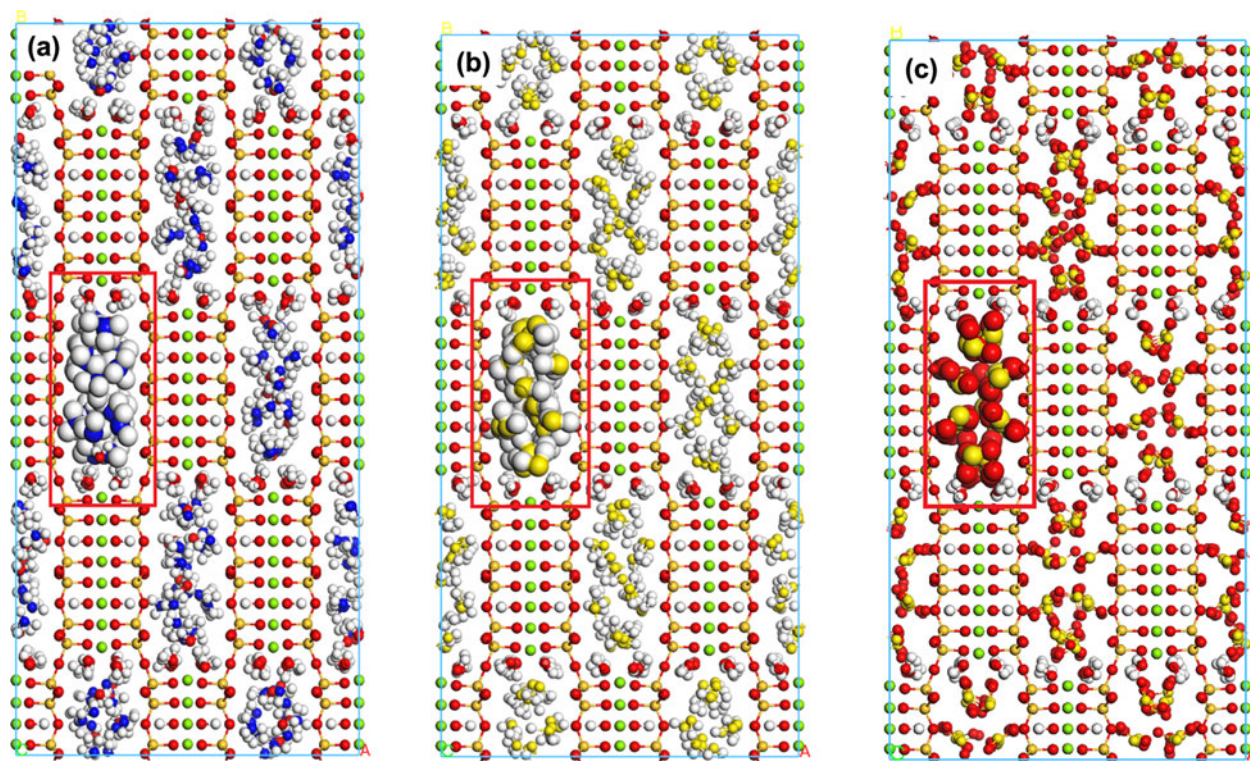


**Fig. 4.** Snapshots of the molecular configurations of the gases in the channels after relaxation at  $\chi_4 = 2.0$ , where N is represented by the blue balls, S is represented by the yellow balls, O is represented by the red balls, H is represented by the grey balls and Mg is represented by the green balls. (a)  $\text{NH}_3$  model; (b)  $\text{H}_2\text{S}$  model; and (c)  $\text{SO}_2$  model.

configurations. The  $\text{H}_2\text{S}$  and  $\text{SO}_2$  molecules exhibited ring-like structures in the channels.

The stability of the adsorption was evaluated using the diffusion coefficients of the gas molecules, and the results are shown in Table 2 (Zhou *et al.*, 2016; Largo *et al.*, 2020). For  $\text{NH}_3$ , the diffusion coefficient of the molecules in the channel was  $0.53 \times 10^{-9} \text{ m}^2 \text{ s}^{-1}$  at  $\chi_1 = 0.2$ , which decreased to  $0.17 \times 10^{-9} \text{ m}^2 \text{ s}^{-1}$  at  $\chi_2 = 0.5$ . When  $\chi_3$  increased continuously to 1.0, the diffusion coefficient increased slightly and then declined to  $0.17 \times 10^{-9} \text{ m}^2 \text{ s}^{-1}$  at  $\chi_4 = 2.0$ . The relatively high diffusion coefficient indicates a weak interaction between  $\text{NH}_3$  molecules and sepiolite. The change in the  $\text{H}_2\text{S}$  diffusion coefficient was similar to that observed for  $\text{NH}_3$ , which indicates that the adsorption of  $\text{H}_2\text{S}$  molecules is related to the

number of zeolitic water molecules. At  $\chi_1 = 2.0$ , the diffusion coefficient of  $\text{H}_2\text{S}$  was  $0.50 \times 10^{-12} \text{ m}^2 \text{ s}^{-1}$ , which was three orders of magnitude lower than that at  $\chi_1 = 0.2$ . This indicates that sepiolite shows a great adsorption ability towards  $\text{H}_2\text{S}$ . In comparison, the diffusion coefficients of  $\text{SO}_2$  and  $\text{H}_2\text{O}$  decreased gradually with increasing  $\chi_i$ , which could be ascribed to the strong interaction between  $\text{SO}_2$  and the walls of the channel. In addition, the diffusion coefficients of  $\text{SO}_2$  were an order of magnitude lower than those of  $\text{H}_2\text{S}$ , suggesting a greater adsorption ability for  $\text{SO}_2$  in sepiolite. At  $\chi_4 = 2.0$ , the diffusion coefficients of structural water molecules for both  $\text{H}_2\text{S}$  and  $\text{SO}_2$  were also similar, which is in agreement with the molecular configurations shown in Fig. 4.

**Table 2.** Diffusion coefficients of the gas molecules in the channels of the computational model.

Model	$\chi_i$	$D_{\text{gas}}$ ( $10^{-9} \text{ m}^2 \text{ s}^{-1}$ )	$D_{\text{water}}$ ( $10^{-9} \text{ m}^2 \text{ s}^{-1}$ )
$\text{NH}_3$	$\chi_1 = 0.2$	0.53	0.40
	$\chi_2 = 0.5$	0.17	0.15
	$\chi_3 = 1.0$	0.20	0.10
	$\chi_4 = 2.0$	0.17	0.10
	$\chi_1 = 0.2$	0.13	0.15
$\text{H}_2\text{S}$	$\chi_2 = 0.5$	0.0043	0.0041
	$\chi_3 = 1.0$	0.0064	0.0039
	$\chi_4 = 2.0$	0.0050	0.0013
	$\chi_1 = 0.2$	0.032	0.048
$\text{SO}_2$	$\chi_2 = 0.5$	0.0049	0.0097
	$\chi_3 = 1.0$	0.0016	0.0016
	$\chi_4 = 2.0$	0.00064	0.0011

## Conclusions

MD simulations have been employed successfully to study the adsorption mechanism of hazardous gases such as  $\text{NH}_3$ ,  $\text{H}_2\text{S}$  and  $\text{SO}_2$  on sepiolite. Upon calculation of the distribution and diffusion coefficients of the gas molecules in the channels of sepiolite, it was found that the adsorption ability of sepiolite for the three gases followed the order  $\text{SO}_2 > \text{H}_2\text{S} > \text{NH}_3$ . While the  $\text{NH}_3$  molecules in the channels exhibited great affinity for the water molecules, and  $\text{H}_2\text{S}$  molecules showed strong interactions with the water molecules and the walls of the channels. The  $\text{SO}_2$  molecules exhibited strong interactions with both the Si atoms in sepiolite and the O atoms in structural water. Thus, it was found that the atomic configuration of the gas molecules in the channels are affected by both  $\chi_i$  and the interactions between the gas molecules and sepiolite. Additionally, ring-like structures are observed in the molecular configurations of  $\text{H}_2\text{S}$  and  $\text{SO}_2$ . Future experiments will be required to validate these findings.

**Financial support.** This work was financially supported by the Natural Science Foundation of Hunan Province (No. 2019JJ40093) and the High-Level Talent Gathering Project in Hunan Province (No. 2019RS1059). ACSA also thanks the CNPq (425730/2018-2) and FAPEMA (00961/18).

**Conflicts of interest.** The authors declare that they have no conflicts of interest.

**Supplementary material.** To view supplementary material for this article, please visit <https://doi.org/10.1180/clm.2022.22>.

## References

- Abbaspour M., Akbarzadeh H. & Valizadeh Z. (2018) Au–Ir nanoalloy nucleation during the gas-phase condensation: a comprehensive MD study including different effects. *Inorganic Chemistry Frontiers*, **5**, 1445–1457.
- Alcántara A.C., Darder M., Aranda P. & Ruiz-Hitzky E. (2012) Zein–fibrous clays biohybrid materials. *European Journal of Inorganic Chemistry*, **2012**, 5216–5224.
- Alver B.E. (2018) Hydrogen adsorption on natural and sulphuric acid treated sepiolite and bentonite. *International Journal of Hydrogen Energy*, **43**, 831–838.
- Balci S. (1999) Effect of heating and acid pre-treatment on pore size distribution of sepiolite. *Clay Minerals*, **34**, 647–655.
- Bashir S., Ali U., Shaaban M., Gulshan A.B., Iqbal J., Khan S. et al. (2020) Role of sepiolite for cadmium (Cd) polluted soil restoration and spinach growth in wastewater irrigated agricultural soil. *Journal of Environmental Management*, **258**, 110020.
- Cecilia J., Vilarrasa-García E., Cavalcante Jr C., Azevedo D., Franco F. & Rodríguez-Castellón E. (2018) Evaluation of two fibrous clay minerals (sepiolite and palygorskite) for CO<sub>2</sub> capture. *Journal of Environmental Chemical Engineering*, **6**, 4573–4587.
- Cornejo J. & Hermosin M. (1988) Structural alteration of sepiolite by dry grinding. *Clay Minerals*, **23**, 391–398.
- Delgado J.A., Uguina M.A., Sotelo J.L., Ruiz B. & Rosário M. (2007) Carbon dioxide/methane separation by adsorption on sepiolite. *Journal of Natural Gas Chemistry*, **16**, 235–243.
- Deng C., Jiang Y., Fan Z., Zhao S., Ouyang D., Tan J. et al. (2019) Sepiolite-based separator for advanced Li-ion batteries. *Applied Surface Science*, **484**, 446–452.
- Erdoğan B. & Esenli F. (2022) Sepiolite as an efficient adsorbent for ethylene gas. *Clay Minerals*, **56**, 222–228.
- Fayazi M., Afzali D., Ghanei-Motlagh R. & Irajli A. (2019) Synthesis of novel sepiolite–iron oxide–manganese dioxide nanocomposite and application for lead (II) removal from aqueous solutions. *Environmental Science and Pollution Research*, **26**, 18893–18903.
- Fitaroni L.B., Venâncio T., Tanaka F.H., Gimenez J.C., Costa J.A. & Cruz S.A. (2019) Organically modified sepiolite: thermal treatment and chemical and morphological properties. *Applied Clay Science*, **179**, 105149.
- García-Romero E. & Suárez M. (2013) Sepiolite–palygorskite: textural study and genetic considerations. *Applied Clay Science*, **86**, 129–144.
- García-Romero E. & Suárez M. (2018) A structure-based argument for non-classical crystal growth in natural clay minerals. *Mineralogical Magazine*, **82**, 171–180.
- Hamid Y., Tang L., Hussain B., Usman M., Liu L., Ulhassan Z. et al. (2021) Sepiolite clay: a review of its applications to immobilize toxic metals in contaminated soils and its implications in soil–plant system. *Environmental Technology & Innovation*, **23**, 101598.
- He L., Li G., Lv S., Gao J., Kowalski K.J., Valentin J. & Alexiadis A. (2020) Self-healing behavior of asphalt system based on molecular dynamics simulation. *Construction and Building Materials*, **254**, 119225.
- Jiang W., Jiang Y., Zhao S., Peng J., Qin W., Ouyang D. & Ding Y. (2020) Novel sepiolite-based materials for lithium- and sodium-ion storage. *Energy Technology*, **8**, 1901262.
- Jiang W., Han Y., Jiang Y., Xu F., Ouyang D., Sun J. et al. (2021) Preparation and electrochemical properties of sepiolite supported Co<sub>3</sub>O<sub>4</sub> nanoparticles. *Applied Clay Science*, **203**, 106020.
- Kitayama Y. & Hayakawa M. (1992) Elimination of impurity in sepiolite and its surface area. *Journal of the Clay Science Society of Japan*, **31**, 196–201 (in Japanese).
- Lamichhane T.R. & Ghimire M.P. (2021) Evaluation of SARS-CoV-2 main protease and inhibitor interactions using dihedral angle distributions and radial distribution function. *Heliyon*, **7**, e08220.
- Largo F., Haounati R., Akhouairi S., Ouachtak H., El Haouti R., El Guerdaoui A. et al. (2020) Adsorptive removal of both cationic and anionic dyes by using sepiolite clay mineral as adsorbent: experimental and molecular dynamic simulation studies. *Journal of Molecular Liquids*, **318**, 114247.
- Lu Y. & Wang A. (2022) From structure evolution of palygorskite to functional material: a review. *Microporous and Mesoporous Materials*, **333**, 111765.
- Muniz-Miranda F., Lodesani F., Tavanti F., Presti D., Malferrari D. & Pedone A. (2016) Supercritical CO<sub>2</sub> confined in palygorskite and sepiolite minerals: a classical molecular dynamics investigation. *Journal of Physical Chemistry C*, **120**, 26945–26954.
- Qiu P., Guo L., Qi Y., Cheng M. & Jing Z. (2021) Hydrothermal solidification of sepiolite into a cemented sepiolite aggregate for humidity regulation and formaldehyde removal. *Clay Minerals*, **55**, 320–328.
- Sabah E., Çınar M. & Çelik M.S. (2007) Decolorization of vegetable oils: adsorption mechanism of β-carotene on acid-activated sepiolite. *Food Chemistry*, **100**, 1661–1668.
- Suárez M. & García-Romero E. (2013) Sepiolite–palygorskite: a continuous polysomatic series. *Clays and Clay Minerals*, **61**, 461–472.
- Sun T., Xiao J.J., Liu Q., Zhao F. & Xiao H.M. (2014) Comparative study on structure, energetic and mechanical properties of a ε-CL-20/HMX cocrystal and its composite with molecular dynamics simulation. *Journal of Materials Chemistry A*, **2**, 13898–13904.
- Yebrá-Rodríguez A., Martín-Ramos J.D., Del Rey F., Viseras C. & López-Galindo A. (2003) Effect of acid treatment on the structure of sepiolite. *Clay Minerals*, **38**, 353–360.
- Yuan M., Gao G., Hu X., Luo X., Huang Y., Jin B. & Liang Z. (2018) Premodified sepiolite functionalized with triethylenetetramine as an effective and inexpensive adsorbent for CO<sub>2</sub> capture. *Industrial & Engineering Chemistry Research*, **57**, 6189–6200.
- Zheng S.-Q., Han Y., Huang X.-H., Dai Y.-L., Qian D., Zhang J.-C. & Ren S. (2010) Acid and aluminium modification of sepiolite and its application in FCC catalysis. *Clay Minerals*, **45**, 15–22.
- Zhou J., Lu X. & Boek E.S. (2016) Confined water in tunnel nanopores of sepiolite: insights from molecular simulations. *American Mineralogist*, **101**, 713–718.